Available online at www.sciencedirect.com

ScienceDirect

Advances in Space Research 62 (2018) 71–83

ADVANCES IN SPACE RESEARCH (a COSPAR publication)

www.elsevier.com/locate/asr

Application of the GNSS-R in tomographic sounding of the Earth atmosphere

Milad Jaberi Shafei [a], Masoud Mashhadi-Hossainali [b,*]

[a] Faculty of Geodesy and Geomatics Engineering, K. N. Toosi University of Technology, Iran
[b] Department of Geodesy, Faculty of Geodesy and Geomatics Engineering, K. N. Toosi University of Technology, Iran

Received 26 April 2017; received in revised form 16 March 2018; accepted 5 April 2018
Available online 14 April 2018

Abstract

Reflected GNSS signals offer a great opportunity for detecting and monitoring of water level variation, land surface roughness and the atmosphere around the Earth. The application type intensely depends on satellites' geometry and the topography of study area. GNSS-R can be used in sounding the water vapor as one of the most important parameters in troposphere. In view of temporal and spatial changes, retrieval of this parameter is complicated. GNSS tomography is a common approach for this purpose. Considering the dependency of this inverse approach to the number of stations and satellites' coverage at study area, tomographic reconstruction of water vapor is an ill-posed problem. Additional constraints are usually used to find a solution. In this research reflected signals known as GNSS-R are offered for the first time to resolve the rank deficiency of this problem. This has been implemented to a tomographic model which has been already developed for modeling the water vapor in the North West of Iran. In view of low number of GPS stations in this area, the design matrix of the model is rank deficient. Simulated results demonstrate that the rank deficiency of this matrix can be reduced by implementing appropriate number of GNSS-R stations when the spatial resolution of model is optimized. Resolution matrix is used as a measure for analyzing the efficiency of the proposed method. Results from DOY 300 and 301 in year 2011 show that the applied method can even remedy the rank deficiency of the design matrix. The satellites' constellation and the time response of the model are the effective parameters in this respect. On average the rank deficiency of the design matrix is improved more than 90% when the reflected signals are used. This is easily seen in terms of the resolution matrix of the model. Here, the mean bias and RMSE of reconstructed image are 0.2593 and 1.847 ppm, respectively.

Keywords: GNSS tomography; GNSS-R; Rank deficiency; Resolution matrix

1. Introduction

For over decades, Global Navigation Satellite Systems are used in various applications to remotely sense the earth. In most cases, the interference of direct and reflected signals remains a major problem (multipath effect). First time the idea of using reflected signals to extract various parameters of the surface was proposed by Martin-Neira (1993). This remote sensing technique known as GNSS Reflectometry is based on using reflected signals (Fig. 1). Today, several parameters of the reflecting surface can be retrieved by using the delay between the direct signal (received by zenith-looking antenna) and reflected signal (received by nadir-looking antenna) or by analyzing the waveforms (temporal evolution of the signal power) corresponding to the reflected signal. In most cases the difference between the direct and reflected signal is about a few wave peaks for ground-based and air-borne campaigns. This advantage can be interpreted in terms of altimetry which

* Corresponding author.
E-mail addresses: m.jaberi@email.kntu.ac.ir (M. Jaberi Shafei), hossainali@kntu.ac.ir (M. Mashhadi-Hossainali).

https://doi.org/10.1016/j.asr.2018.04.003
0273-1177/

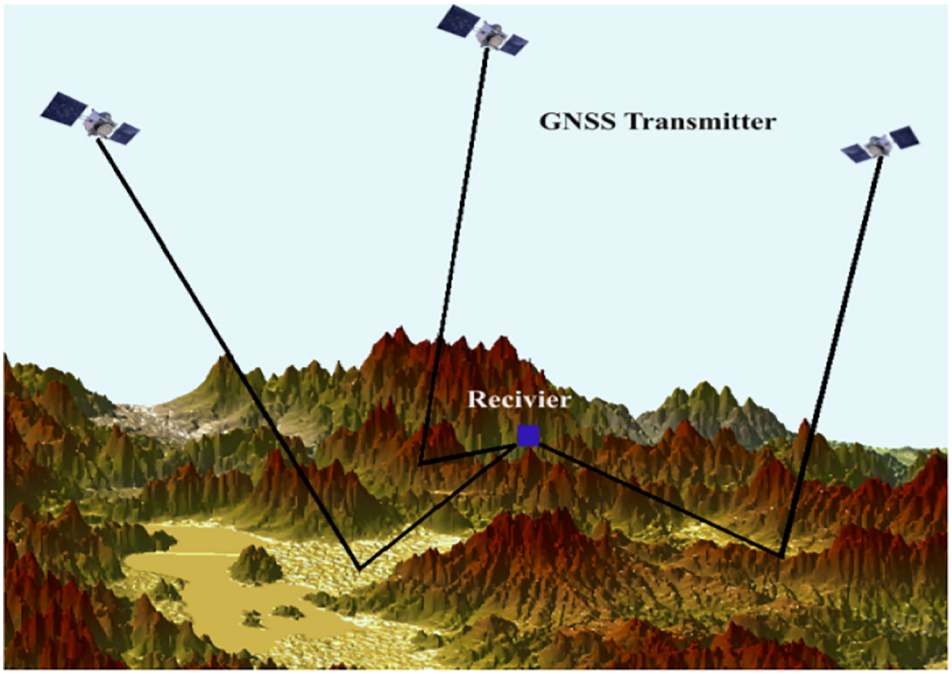

Fig. 1. Geometry of reflectometry in a ground based GNSS-R campaign.

demonstrates the height difference between receiver and the surface below. Temporal variation of the sea surface and the lake level can be obtained by the accuracy of centimeters for ground-based and air-borne receivers (Ruffini et al., 2004; Semmling et al., 2011; Löfgren et al., 2011; Lowe et al., 2002; Rodriguez-Alvarez et al., 2011).

Surface roughness and other parameters such as soil moisture, wave height, wind speed and ice properties can be retrieved from analyzing Delay Doppler Maps (DDM) extracted from the waveforms (Zavorotny and Voronovich, 2000; Rodriguez-Alvarez et al., 2009, 2011; Katzberg et al., 2006). The particular advantage of this technique is the dense temporal and spatial coverage not limited to a single measurement point or a non-repetitive transect as with using classical GNSS buoys (Roussel et al., 2014).

Water vapor is an important parameter to assess the Weather condition in metrology. Large variation of this parameter requires a reconstruction approach that simultaneously takes its spatial and temporal variations into account. GNSS tomography is a technique which makes it possible to obtain a 3D picture of lower (medium) troposphere. It also probes wet refractivity and water vapor distribution in space and time (Rohm and Bosy, 2009). In the first instance, tomography was used in medical science in fifty's. Then it was used obtaining geodynamics (Bourjot and Romanowicz, 1992), gas tracing (Degaleesan et al., 2001), ionosphere reconstruction (Thampi et al., 2009) and tropospheric reconstruction with GNSS signal. The advantage of tropospheric reconstruction of water vapor compared to other methods is working in all-weather condition with high temporal resolution (Yang et al., 1999).

Water vapor tomography is implemented with a finite number of 3D elements (voxels) with assumed constant unknown values. Water vapor values are then obtained by tracing the GNSS signals passing through the elements (Adavi and Mashhadi-Hossainali, 2014; Bi et al., 2006; Rohm and Bosy, 2009). The GNSS satellites' geometry is not appropriate for this inverse problem. In addition to that, when the spatio-temporal variation of the desired parameter is high and/or the number and spatial distribution of the GNSS stations is not sufficient within the study area, GNSS signals cannot constrain the model; giving an under determined problem (Champollion et al., 2005).

Several methods have been devised in order to reduce the rank deficiency or to constrain a tomography model. Hirahara (2000) proposed additional horizontal and vertical smoothing equation to solve for the inverse solution (Hirahara, 2000). Flores et al. (2001) applied additional constraints in the form of a Kalman filter to the tomographic problem and gained the solution (Flores et al., 2001). Nilsson and Gradinarsky (2006) found the solution directly from GPS phase measurement equation (Nilsson and Gradinarsky, 2006). Bender et al. (2011) used algebraic reconstruction method to solve the problem. They used radiosonde and surface measurements to constrain the problem (Bender et al., 2011). Radiosonde and radio occultation profiles are two independent sets of constraints which have also been used for resolving the rank deficiency of this problem (Xia et al., 2013; Foelsche and Kirchengast, 2001; Bender et al., 2011; Bi et al., 2006). Adavi and Mashhadi-Hossainali (2014) applied the idea of using Virtual Reference Stations as the required constraints (Adavi and Mashhadi-Hossainali, 2014). This research proposes

the application of reflected signals to constraint a tomography model. The specular points' position plays a key role in this respect.

The next section of this paper discusses on the tomographic approach for troposphere modeling. Applied method for determining the specular points' position is then described. The concept of resolution matrix is used in order to analyze the efficiency of using reflected signals in constraining the tomographic model of this research. In the final section, study area is introduced and also numerical results and the corresponding discussions are given.

2. Methodology

Here, the concept of troposphere tomography is firstly introduced. Then specular point position calculation is briefly described. Finally, resolution matrix and its application to tomographic model are given.

2.1. Troposphere tomography

Slant tropospheric delay for GPS signal can be retrieved by the equation below (Bevis et al., 1992):

$$STD = 10^{-6} \int N\, ds \tag{1}$$

Here, ds is the differential length element between transmitter and receiver and N is the refractivity parameter. By using dry and wet components of tropospheric delay, Eq. (1) can be rewritten as the sum of slant hydrostatic and wet delays:

$$STD = (\mathrm{SHD} + \mathrm{SWD}) = 10^{-6} \int (N_d + N_w) ds \tag{2}$$

In equation above, N_d and N_W represent the dry and wet components of refractivity, respectively. Moreover, SHD is the hydrostatic and SWD is the wet slant delay. Calculating the dry component and subtracting it from the total slant delay, the slant wet delay is derived as equation below:

$$SWD = 10^{-6} \int N_w\, ds \tag{3}$$

Eq. (3) is the observation equation in GPS troposphere tomography. Since the signal path is a function of the wet refractivity field, the observation equation is nonlinear. The equation is linearized assuming that the GPS signal is transmitted in a straight line. Thus for implementation, Eq. (3) is substituted by the discrete form as given below:

$$SWD_i = 10^{-6} \sum N_{wj} \Delta s_j \tag{4}$$

where j & Δs_j represent the voxel number that the emitted signal passes through and the signal length in that element. In matrix notation, Eq. (4) is written in the following form:

$$\mathbf{d} = \mathbf{A}\mathbf{p} \tag{5}$$

Here, $\mathbf{d}$ is the vector of the slant wet delays, $\mathbf{p}$ is the vector of unknown parameters (N_{wj}) and $\mathbf{A}$ is the design matrix with $m \times n$ dimensions:

$$\mathbf{A} = \begin{bmatrix} d_{11} & . & . & . & d_{1n} \\ d_{21} & . & . & . & d_{2n} \\ . & . & . & . & . \\ . & . & . & . & . \\ d_{m1} & . & . & . & d_{mn} \end{bmatrix} \tag{6}$$

m is the number of SWDs observed in each epoch and n is the number of voxels. The parameter m depends on the selected time response for the model as well as the number of GPS stations and the number of the GPS visible satellites.

In matrix above d_{ij} is the length of the ith ray within the jth element of the tomographic model. If the ray does not intersect a voxel, the related element is set to zero. Moreover, the refraction of the signal is ignored (Adavi and Mashhadi-Hossainali, 2014; Rohm and Bosy, 2009; Troller et al., 2006). Matrix $\mathbf{A}$ reflects the experiments physics and geometry. Therefore, the spatial discretization; i.e. the choice of a specific grid is an important issue and depends on several parameters. One of the principal matters for troposphere modeling and wet delay reconstruction is the spatial and temporal correlation distance of the tropospheric wet refractive component. If the voxel sizes were larger than the tropospheric spatial correlation radius, realistic image of the tropospheric parameters could not be reconstructed by the model. On the other hand, the geometry of the ranging sources can yield sharp increase in the inverted design matrix. Improperly selected positions for transmitters (sources) and/or receivers can increase the instability of a tomographic solution. In GNSS tomography, GNSS satellites are the transmitters and GNSS antennas are the receivers. Here, the transmitters-receivers' geometry cannot be changed. As the result, the geometry of the ranging sources can be controlled through the appropriate selection of ranging sources which do not increase the instability of solution. In practice, the choice of specific grid is made based on the desired application (Guerova et al., 2016). In this regard, it is important that the magnitude of the horizontal grid should not be smaller than the mean interstation distances in study area (Guerova et al., 2016). The vertical resolution is always chosen to increase with height from the ground to the top layer of the model. In order to make a reasonable answer, the vertical resolution for lower layers are chosen between 200 and 500 m and this increases to 1 km for heights that the water vapor component is low (Guerova et al., 2016). In many researches the Numerical Weather Prediction (NWP) models are used to extract the vertical resolution. The height of the model elements is usually 3 to 5 times smaller than the horizontal one (Bosy et al., 2010).

As far as the geometry of the model is concerned, to come up with a unique solution, transmitted signals necessarily should pass through all of the model elements. In

practice, some of the voxels are not constrained by the GPS signals at all while some of the others are passed by more than one signal. Consequently, troposphere tomography is a mixed-determined problem (Menke, 2012).

2.2. Constraining the model by GNSS-R

GNSS-R is a bi-static radar system in which the transmitter and receiver are separated by a significant distance. The first concept was investigated by Martin-Neira (1993) as a method to densify the earth observation in a low cost efficient way: an antenna pointing to transmitter receives the so-called direct rays and an antenna pointing to the surface gathers the signals scattered from the surface of the Earth. Reflected signals have different contributes due to the receiver height. Signal to noise ratio (SNR) for the ground and air-borne receivers is more considerable as compared to the space-borne campaigns (Rius et al., 2010). In GNSS-R technique finding the specular point position is of great interest because the corresponding reflected signal has more power. Proposed methods for finding the specular point position includes local plane, local sphere. Ellipsoidal or the DEM (Digital Elevation Model) integrated approximation as illustrated in Fig. 2.

In order to get a more accurate reflection point we have to take the Digital Elevation Model (DEM) into account (Roussel et al., 2014). The visibility of the receiver from the satellite is a prerequisite in this technique. On the assumption that the signal passes through the space in straight line, the ellipsoidal height is interpolated along the ray path using bilinear or cubic method (Roussel et al., 2014). Here, this is done with respect to a DEM whose resolution is 30 m. Moreover, both methods are used in this research. The GPS stations' height are used to check the interpolation process. Obtained results show millimetric to 3 m differences in flat and mountainous areas, respectively. If the satellite signal intersected the DEM, the receiver would not be visible. Otherwise, the reflection point is assumed to be in the plane that is defined by transmitter, receiver and the center of the Earth. The entire segment of the topographic profile that is located in this plane is checked for the existence of specular points. For this purpose, the following correction is computed for the starting and the ending points of the segments that construct the desired profile (Roussel et al., 2014):

$$d\mathbf{r}(t) = \frac{(\mathbf{r}_s(t) - \mathbf{r}_t(t))}{|\mathbf{r}_s(t) - \mathbf{r}_t(t)|} + \frac{(\mathbf{r}_r(t) - \mathbf{r}_s(t))}{|\mathbf{r}_r(t) - \mathbf{r}_s(t)|} \tag{7}$$

where $\mathbf{r}_s(t)$, $\mathbf{r}_r(t)$ and $\mathbf{r}_t(t)$ are the specular point approximate, the receiver and the transmitter positions, respectively. Eq. (7) is considered then for each segment extremes. If the correction is in the satellite direction, the sign is considered positive, and negative if it is in the receiver direction. In case the sign is the same for two extreme points, there is no reflection point on this segment. Otherwise, we consider the middle of the segment as a new point. Then Eq. (7) is considered for each of the three (extreme and middle) points. The algorithm continues using the same principle explained above till the local normal converges the bisect of the angle between the receiver, transmitter and calculated specular point. This criterion is met within the required tolerance level. Once the reflection point is determined the visibility is checked again.

2.3. Geometric evaluation of the tomographic model

The concept of resolution matrix is an appropriate way to characterize the bias in a discrete inverse problem. In other words, on the assumption that there are no errors in input data (**d**) it is possible to analyze how close the inverse solution is to an original model, by multiplying the generalized inverse of $\mathbf{A}(\mathbf{A}_\dagger)$ with input data, least square solution ($\mathbf{m}_\dagger$) is then derived:

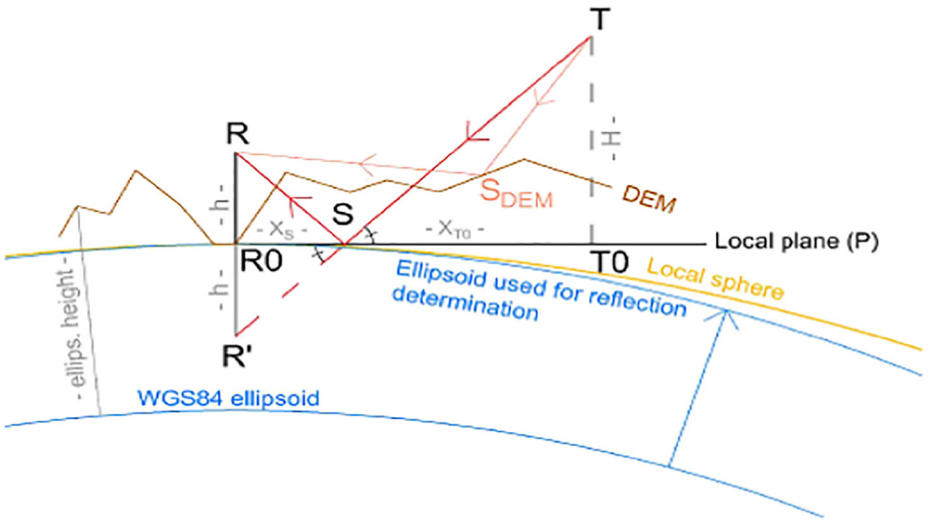

Fig. 2. Different methods for the calculation of reflection point: R is the receiver, T is the transmitter and S is the specular point position (Roussel et al., 2014).

$$\mathbf{m}_{\dagger} = \mathbf{A}_{\dagger}\mathbf{A}\mathbf{m} \tag{8}$$

The product $\mathbf{A}_{\dagger}\mathbf{A}$ which is known as the model resolution ($\mathbf{R}_m$) (Aster et al., 2005) measures how the inverse solution smears out the original model:

$$\mathbf{R}_m = \mathbf{A}_{\dagger}\mathbf{A} \tag{9}$$

Using the spectral decomposition of matrix $\mathbf{A}$, the model space resolution matrix is given by (Watkins, 2002):

$$\mathbf{R}_m = \mathbf{V}_p\mathbf{V}_p^T \tag{10}$$

where p is the number of the singular values which are effectively non-zero and V is the right singular matrix of the coefficient matrix A.

If the rank of the design matrix $\mathbf{A}$ is full the model null space is trivial and $\mathbf{R}_m$ is an identity matrix. In troposphere tomography, this happens if all of the model elements are constrained by GPS signals. Otherwise, i.e. when $rank(\mathbf{A}) = p < n$ or when some of the model elements are not constrained by GPS signals, the resolution matrix is asymmetric with some diagonal elements that are either zero or close to zero. The model parameters that are corresponding to such elements are poorly reconstructed by the inverse solution (Aster et al., 2005).

Based on the previous discussions, the model space resolution concept can provide a priori information on the real improvement in tropospheric reconstruction accuracy and reliability if the model geometry (voxel sizes) properly accounts for the physics and geometry of the problem in the study area. Here, it is already assumed that the voxel sizes have been selected such that the dynamics of the required parameter are taken into account.

3. Numerical results

In this section, at first the study area is introduced. Next, the result of reflection point calculation is described. In the last part, the contribution of the additional constraints is discussed. Through the analysis of the resolution matrix the optimum number of GPS-R stations required in this model is also given.

3.1. Study area

In view of the dense GPS network, North West of Iran is considered as the study area. The area contains 15 operational GPS stations, 10 synoptic stations and one radiosonde station in the selected time period of this research (Fig. 3). A tomographic model has been already designed for the reconstruction of water vapor here too (Adavi and Mashhadi-Hossainali, 2014). This model is used in order to analyze the efficiency of reflected signals in constraining this inverse problem. Assumed GNSS-R stations are located where the number and spatial distribution of GPS stations is poor. Moreover, they are positioned at the highest altitudes. This idea is adopted from the mountain based radio occultation technique for extracting the atmospheric parameters (Zuffada et al., 1999). In this study, the height of GPS stations ranges from 1300 to 1930 m above the Mean Sea Level (MSL) while, the height of the GNSS-R stations ranges from 1960 to 3320 m above the MSL. Fig. 4 illustrates the spatial distribution of the GPS and GNSS-R stations in the test field of this research.

The green triangles illustrate the GPS stations and the cyan circles show the assumed reflectometry points. Obviously, the reflectometry stations are located at higher elevations than the surrounding GPS points.

3.2. Calculation of specular points

The algorithm which was outlined in Section 2.2 is used for calculating the position of the reflection points. To this end, only the GPS satellites are taken into account. Precise satellite orbits from the IGS final products known as SP3 files are used. Then an appropriate interpolation method is implemented to gain the satellites' position in 30 s time steps, equal to the sampling rate of measurements in GPS observation files. Reflection point calculator algorithm is used and some of the calculated points are rejected because the ray path between the reflection point and receiver/-transmitter is intersected by DEM. Specular points computed for the GPS signals with elevation angles below 10° and also the reflection points that are located outside of the study area are neglected automatically. Fig. 5 illustrates the position of the calculated reflection points that fulfill the visibility condition. In this figure, the specular point positions are limited to DOYs 300 and 301 in 2011. Reflection points are given relative to the topography of the study area. DEM is used for reconstructing the topography.

Accordingly, the specular point positions depend on the constellation of the GPS satellites in the desired epoch. This is easily seen when Fig. 5a is compared to Fig. 5b. Moreover, the number of reflection points is increased when the satellites are closer to zenith.

3.3. Tomographic model

Tomographic model that is used in this research is the KNTU1. The efficiency of this model in reconstructing the water vapor has been already proved by Adavi and Mashhadi-Hossainali (2014). The vertical resolution of this model is 500 m from surface to 4 km and then, it is reduced to 1 km up to 10 km from the surface of the Earth (Adavi and Mashhadi-Hossainali, 2014). The horizontal resolution of this model is 30 by 40 km. Fig. 5 illustrates the model together with the topography of the test area. As shown in this figure, the topography of the study area has been taken into account when the tomographic model is designed. The existing height difference between the position of the reflectometry stations and the first layer of the model is also remarkable. Fig. 6 illustrates the position of the reflectometry and GPS stations with respect to this

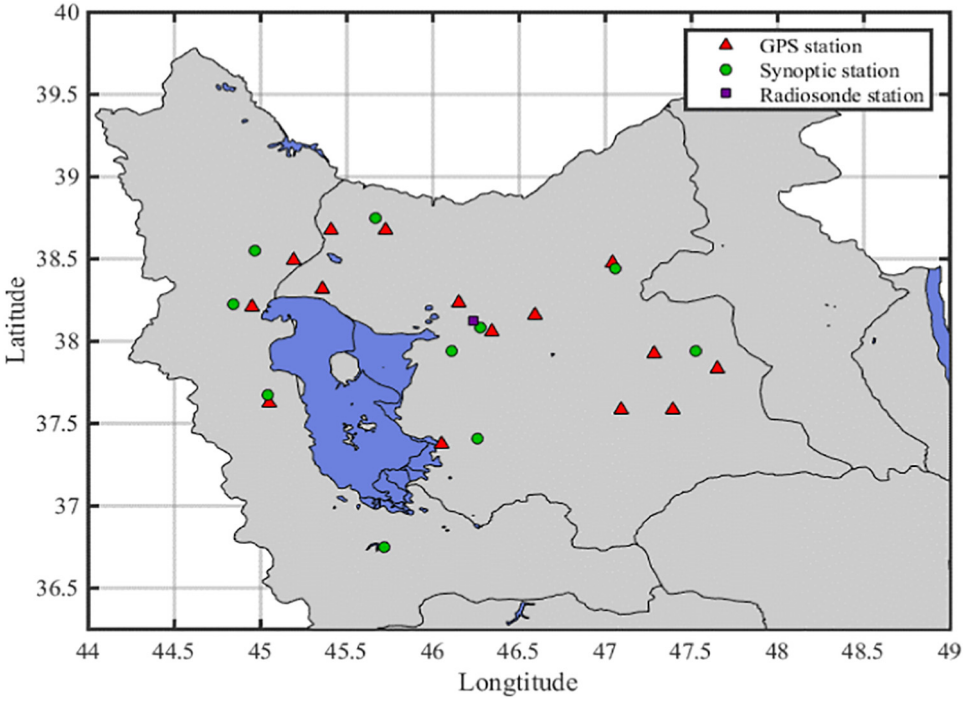

Fig. 3. Distribution of the GPS, Synoptic and radiosonde data in north west of the Iran.

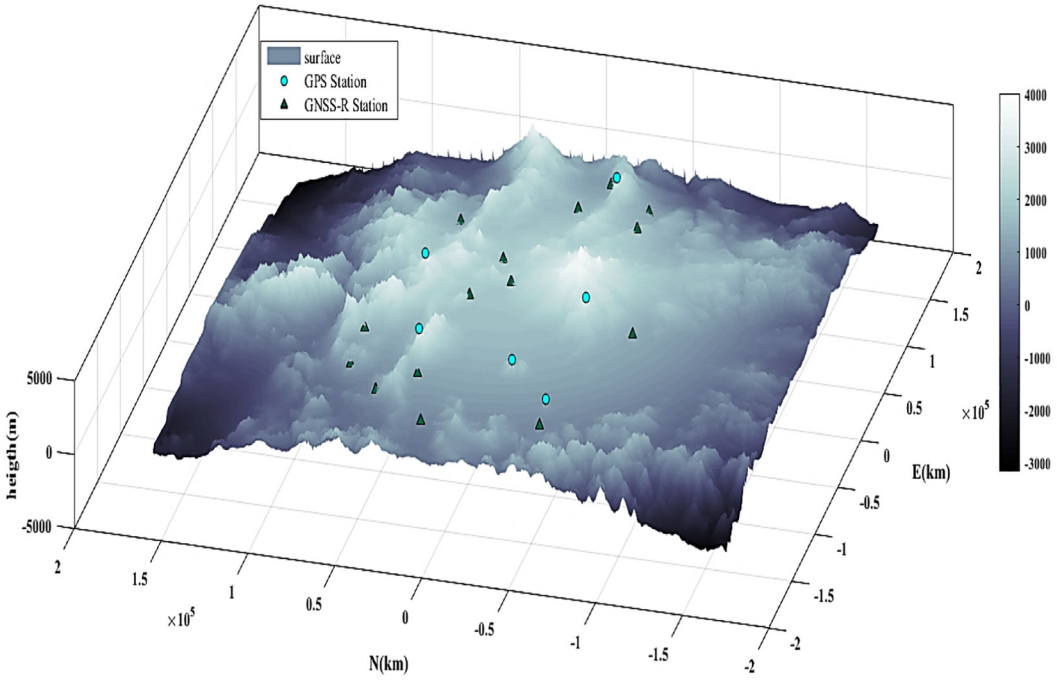

Fig. 4. 3D representation of the study area in North West part of the Iran.

layer of the model. This height difference helps constraining the lower layers of the model more efficiently (see Fig. 7.).

3.4. Numerical evaluation of the model

Design matrix of the model is produced using the ray-tracing algorithm (Bender et al., 2011). The time resolution of the model is one hour. In other words, unknown parameters such as water vapor and/or the wet refractivity are assumed to change in every hour. To obtain the design matrix in the form of Eq. (6), the distance each ray passes through every voxel of the model is determined by solving the intersection of the ray's equation (determined using the positions of transmitter and receiver) with the planes con-

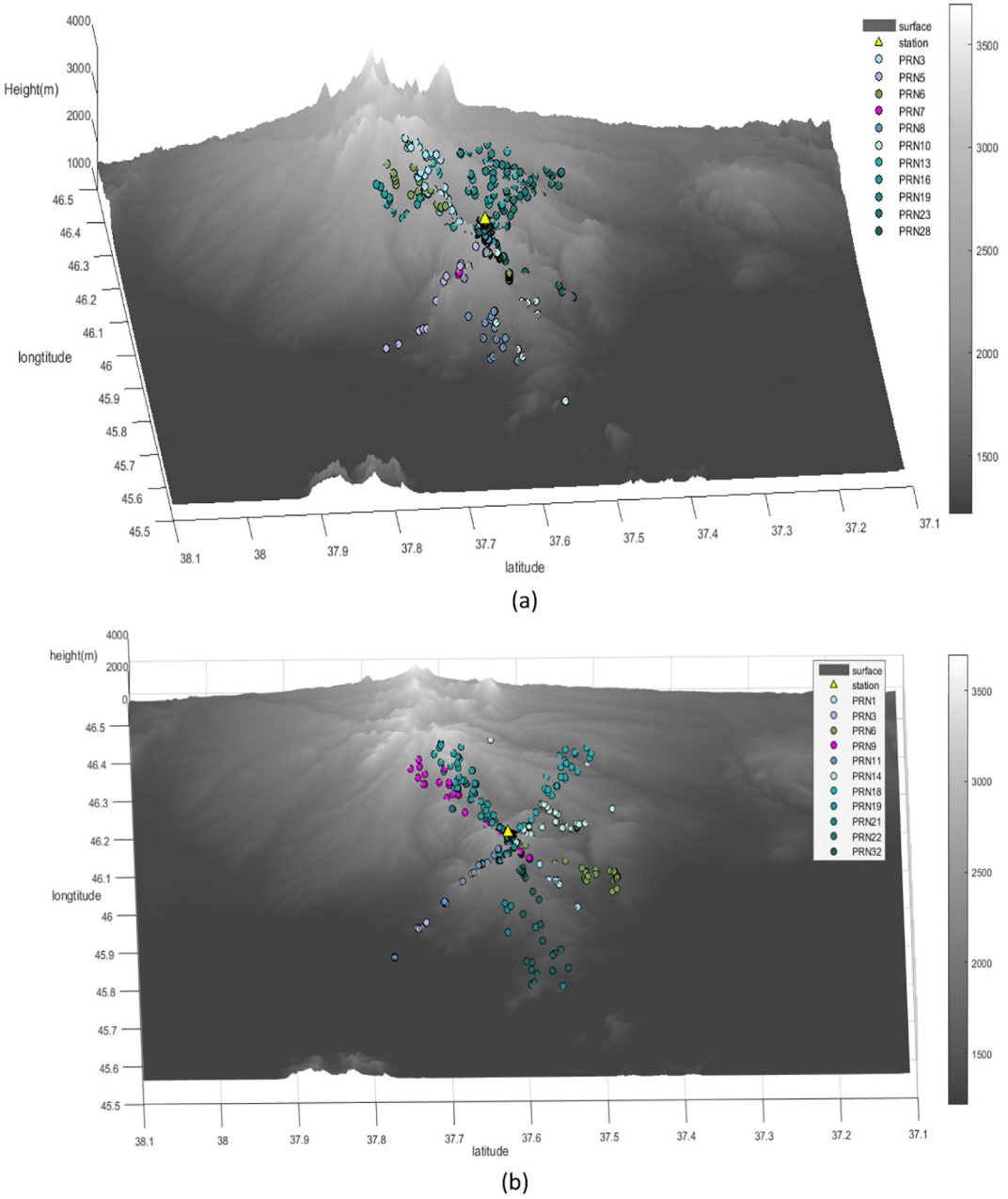

Fig. 5. Calculated reflection points due to DEM for (a) DOY 300, time interval 23–24 in local time and (b) DOY 301, time interval 17–18 in local time.

structing the tomographic model analytically. In KNTU1, this is done in a local Cartesian coordinate frame. The impact of adding reflectometry constraints on the rank of this matrix is analyzed next. Fig. 8 illustrates some of the obtained results. Given results, compare the rank of the design matrix using and without using the GPS-R signals for 12 successive epochs. Here, only 6 GPS-R stations are used for constraining the model.

According to the obtained results, on account that the computed reflection position is not fixed, the impact of reflected signals is not the same even for two similar epochs (see Fig. 8 for further details). This is vividly seen for the 12 h epoch. At this epoch the number of admitted refection point is much fewer than the other epochs (252 versus 3031 at epoch 13 for example). Therefore, at this specific epoch the rank deficiency is reduced less than the others.

In order to analyze the impact of voxel sizes on the required number of GPS-R stations, the horizontal resolution of the model is changed. To this end and following Adavi and Mashhadi-Hossainali (2014), the voxel sizes are reduced to 30 km. The corresponding results are given in Figs. 9–12. The model space resolution matrix is used in order to determine the optimum number of GPS-R stations when the spatial resolution of the model is changed. Results in Fig. 8 show that with five GPS-R stations the rank deficiency is not completely fixed when the spatial resolution of the model is 40 km. It is also not possible to fix the rank deficiency of the problem when the spatial resolu-

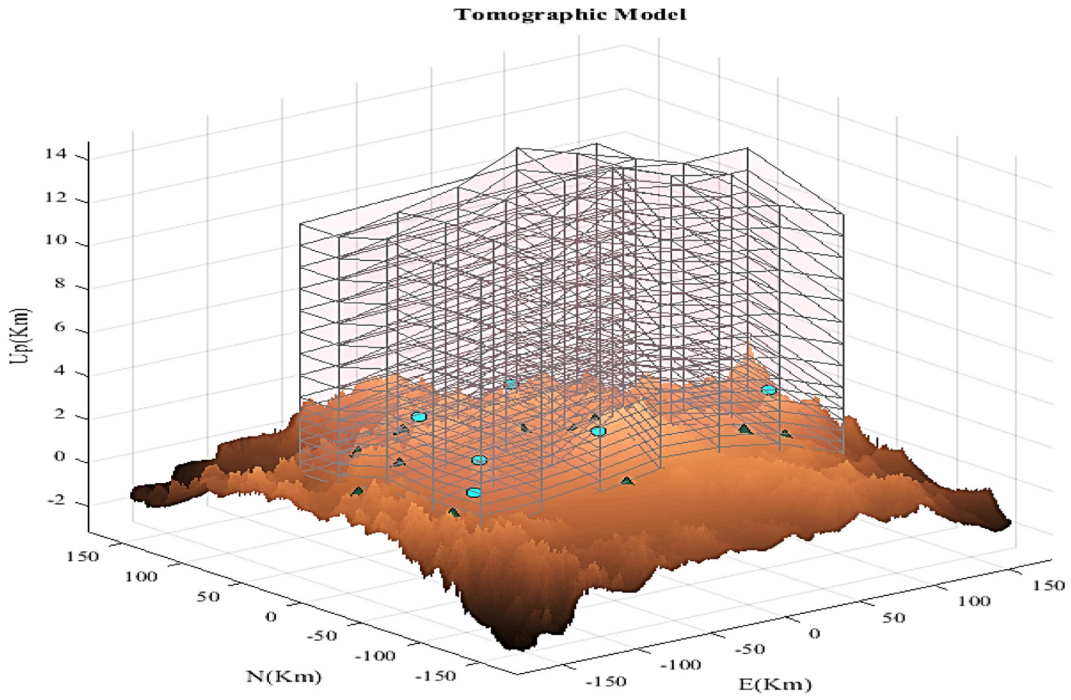

Fig. 6. The KNTU1 model together with the GPS & GPS-R stations as well as the topography of the study area in a local Cartesian coordinate frame.

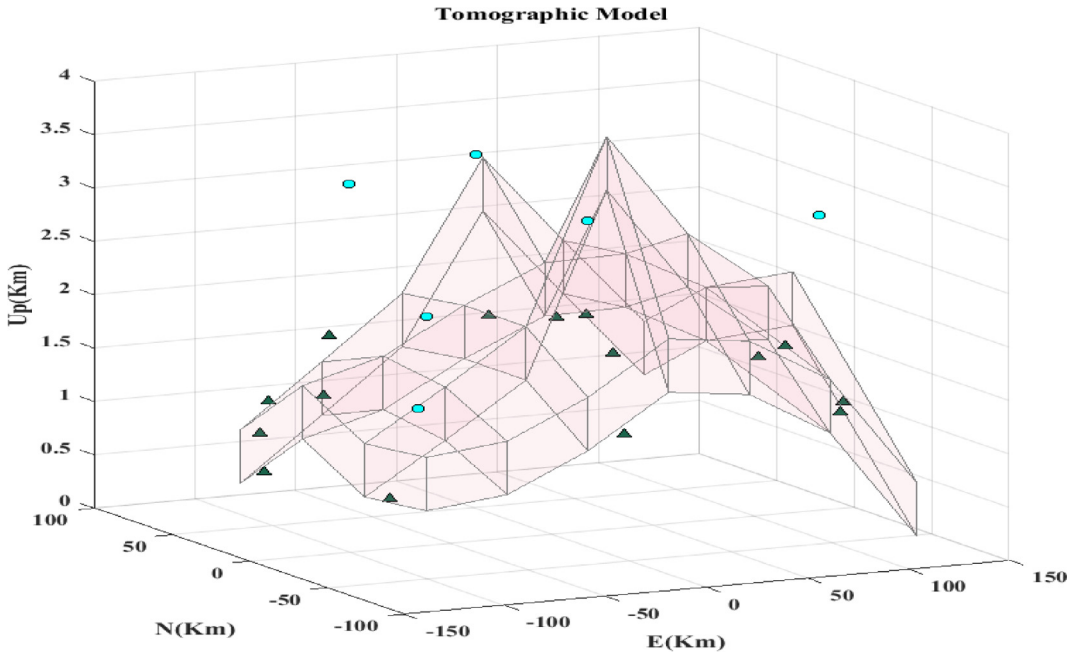

Fig. 7. The relative position of the GPS and GPS-R stations with respect to the first layer of the tomographic model, GPS stations are given by triangles in green, GPS-R stations are shown by cyan circles. The existing height difference between the model and the GPS-R stations helps constraining the lower voxels more efficiently. (For interpretation of the references to colour in this figure legend, the reader is referred to the web version of this article.)

tion is reduced to 30 km. This comparison is also given in Fig. 9: the left three columns illustrate the rank deficiency of the design matrix when the spatial resolution of the model is 40 km and five GPS-R stations are adopted. Next ones give the same parameter for the same spatial resolution but using 6 GPS-R stations. Finally, the right three columns in this figure report on the rank deficiency when the spatial resolution is 30 km and 6 GPS-R stations are applied.

Figs. 10–12 illustrate the application of reflected signals in constraining the model in terms of resolution matrix. According to Figs. 10 and 11, although implementing

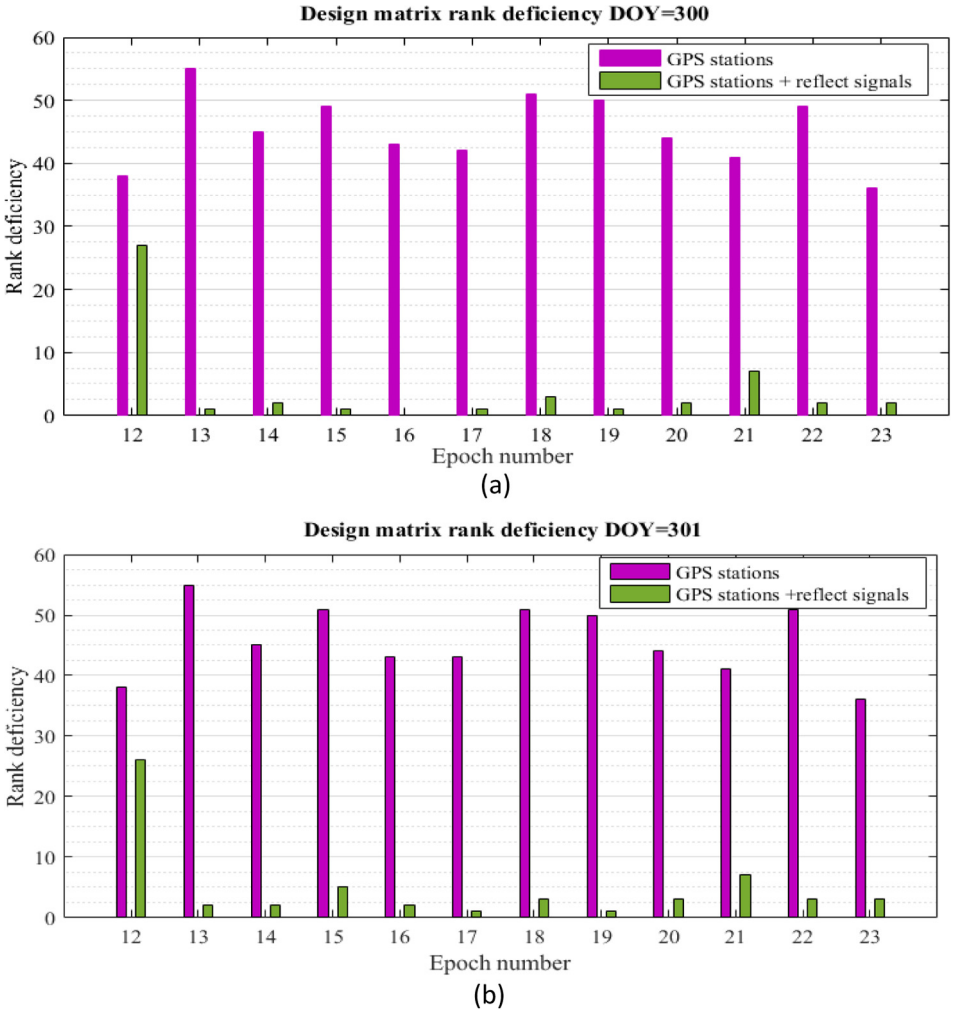

Fig. 8. The impact of using reflected signals on the rank of the design matrix in tomography model of this research, given results are due to DOYs 300 and 301 of the year 2011.

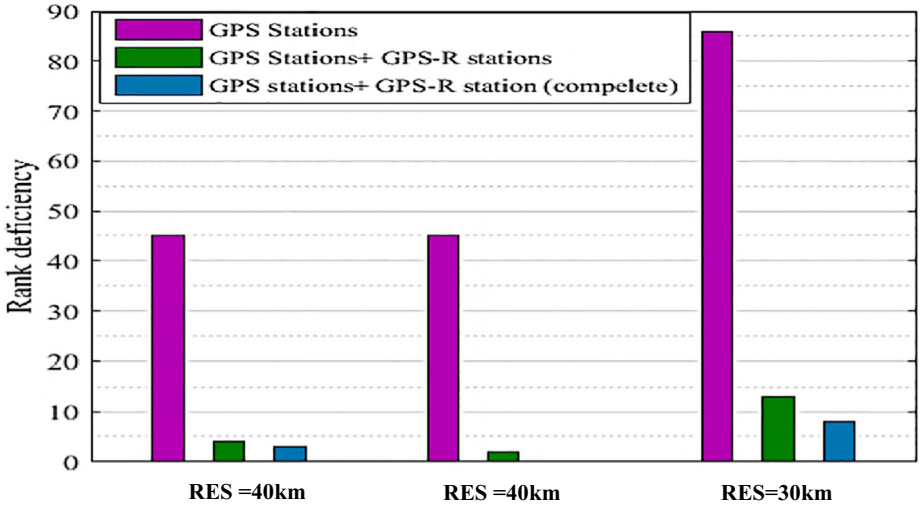

Fig. 9. The influence of reflected signals on the rank of the design matrix for the first epoch (hour 0) of DOY 300 in the year 2011.

reflected signals improves the resolution of the model, some of the voxels steel remain unconstrained. As the result, the resolution matrix is not identity here. This would be at the cost of poor reconstruction of the relevant unknown parameters. Based on Fig. 12 by adding 6 reflectometry points to the GPS stations in this area, the rank deficiency

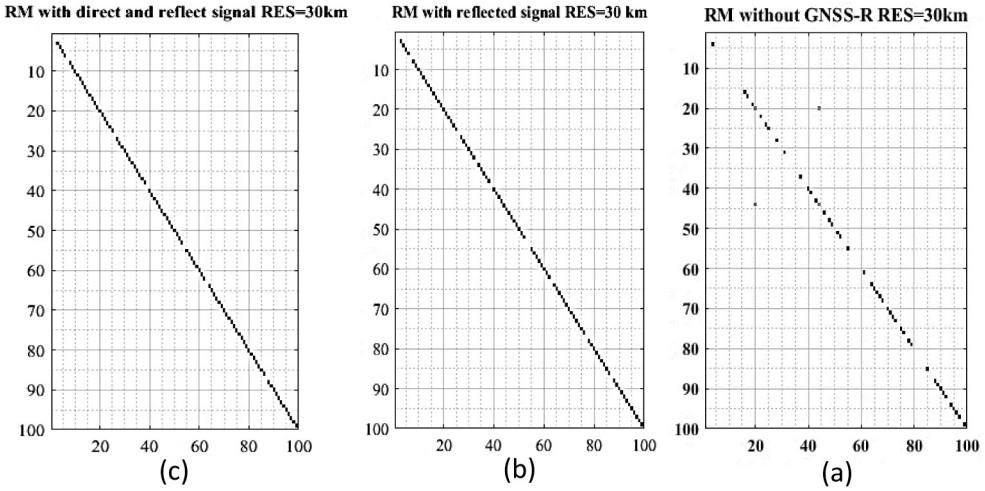

Fig. 10. Resolution Matrix (RM) at the first epoch of the DOY 300. The horizontal resolution of the model is 30 km here: (a) without using GPS-R stations, (b) using reflected signals and (c) with usage of whole GNSS-R concept (reflected signals and direct respectively).

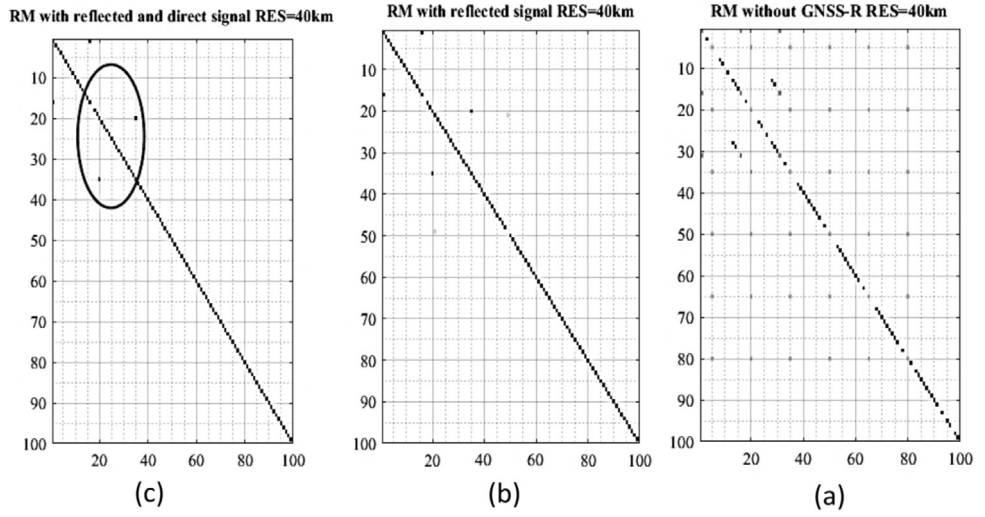

Fig. 11. Resolution matrixes for the first epoch, DOY 300. The horizontal resolution of the mode is 40 km here.

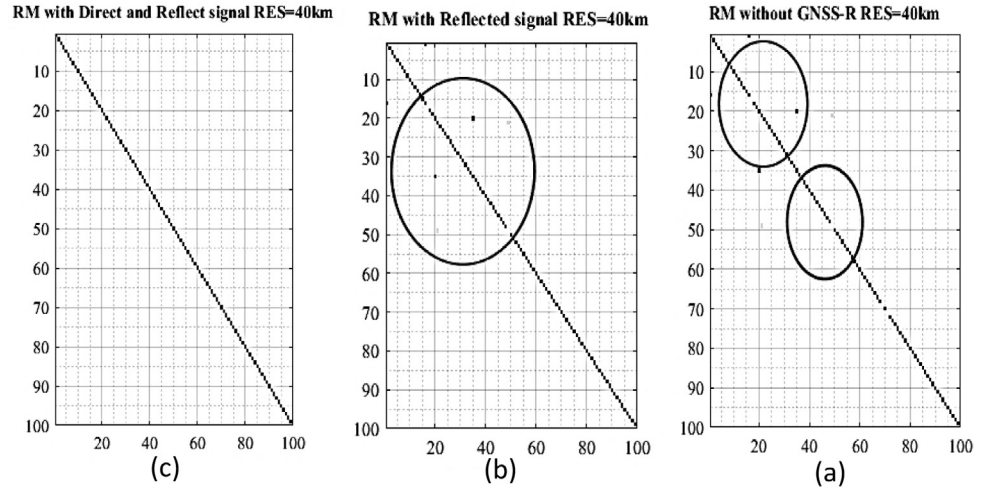

Fig. 12. Resolution matrixes for the first epoch, DOY 300. The horizontal resolution of the model is 40 km.

of the problem can be improved when the spatial resolution of the model is 40 km. Finally, the deficiency is completely repaired by adding the direct rays due to reflected signals.

As compared to the direct signals, the signal to noise ratio is smaller for the GNSS reflected signals. Moreover, the estimation of the tropospheric delay on the reflected signals is still a challenging problem. As the result, the reconstruction errors are expected to be worse when reflected signals are used for constraining a tomographic model. To provide an insight into this problem, the wet refractivity has been reconstructed at and compared to the refractivity profile that is derived from radiosonde measurements in Tabriz. A methodology similar to Adavi and Mashhadi-Hossainali (2014) is preferred and the profile is reconstructed for DOY 300, at 00^{h}:00^{m} in UTC. As the result, reconstructed profile can not only be compared to the radiosonde results, but also is comparable to the profile that is computed using only the direct signals. Both sets of results are reported in Fig. 13. Similar to previous researches [12, 17, 23], the accuracy and precision of the proposed model is analyzed by using The mean bias and Root Mean Squared Error (RMSE) are used for this purpose. These measures are computed using the following equations:

Table 1
Statistical measures computed for the analysis of reconstructed images. The epoch of computation is 00^{h}:00^{m}, DOY 300.Given results are in ppm.

Statistical measures	Using direct and reflected signals	Using direct signals
Mean bias	0.2593	0.0045
RMSE	1.847	1.72

$$RMSE = \sqrt{\frac{1}{N}\sum_{i=1}^{N}(\mathrm{mod}^{i} - cal^{i})^{2}} \tag{11}$$

$$bias = \frac{1}{N}\sum_{i=1}^{N}(\mathrm{mod}^{i} - \mathrm{cal}^{i}) \tag{12}$$

where mod^{i} refers to the parameter that is extracted from tomographic model and cal^{i} is the corresponding radiosonde data at the intended voxels of the model. Calculated measures are given in Table 1. This table also reports the mean bias and the RMSE of the profile which has been already reconstructed using the direct signals.

Given results confirm that the bias and RMSE of reconstructed images are higher as compared to the tomographic images that are reconstructed using the direct signals.

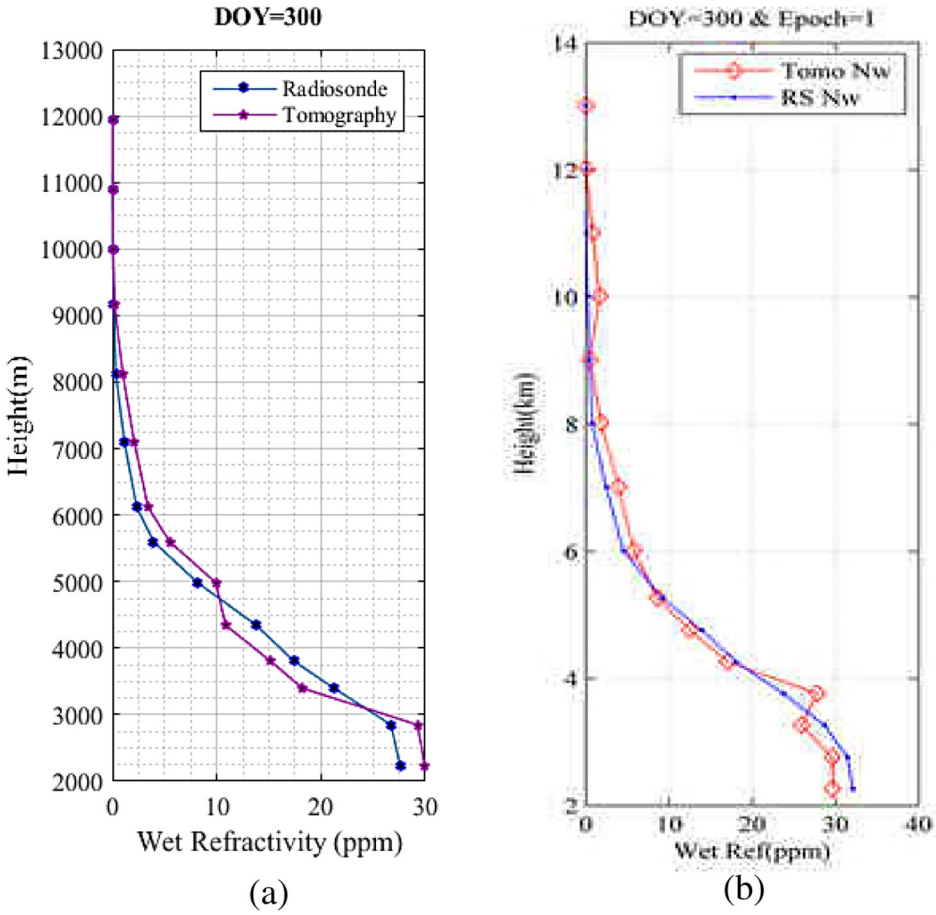

Fig. 13. Comparison of the wet refractivity profile extracted from the direct and reflected signals (a) and the direct only signals (b). Results are associated to the first epoch of DOY 300, 2011.

Increasing the accuracy of the estimated tropospheric delay on reflected signals can help improve the accuracy and precision of the reconstructed image. Nevertheless, the reliability of the obtained results obviously depends on the weather conditions too. For example, in this study the wet refractivity varies from 43.96 to 0.0034 ppm from the surface to the altitude of 19092 m at the Tabriz radiosonde position. This implies that in this study reconstructed wet refractivity is still reliable in terms of the accuracy and precision of the obtained results.

4. Concluding remarks

This study is the first attempt in analyzing the efficiency of the application of reflected signals in constraining a GPS based tomography problem. This is done in a mountainous area located in the North West of the Iran. Two spatial resolutions have been considered for the tomographic model. Starting with 5 GPS-R stations and increasing it to 6, the optimum number of reflectometry points required for constraining the problem has been worked out. Results show that on average reflected signals can reduce the rank deficiency by more than 90%. Based on the obtained results, the satellites' constellation and the time response of the model are the effective parameters in this respect. According to results, implementing reflected signals improves the rank deficiency of the problem but, based on the computed model resolutions; some of the voxels steel remains unconstrained when five GPS-R stations are used. Results show when the spatial resolution is 40 km, by using 6 GPS-R stations the rank deficiency of the model is completely resolved. This is at the cost of increasing the bias and reducing the RMSE of the reconstructed images due to the existing challenge in estimating the tropospheric delay on reflected signals and the higher of reflected signals. Nevertheless, the initial results of this study is promising in the sense that the method is applicable when the humidity is high.

Application of reflected signals in constraining a tomographic model is limited to the space borne, airborne and ground based receiver with significant difference between the reflecting surface and receiver. When the reflection is close to the receiver as in flat areas or when the altitude of the GPS-R receiver is low, the reflected signal is the same as that directly coming to the receiver. As the result, this method will just raise the number of observations without a different impact to the model. In order to obtain more realistic results, simplifications used in this research such as ignoring snow coverage and vegetation should be considered in future researches.

References

Adavi, Z., Mashhadi-Hossainali, M., 2014. 4D tomographic reconstruction of the tropospheric wet refractivity using the concept of virtual reference station, case study: northwest of Iran. Meteorol. Atmos. Phys. 126, 193–205.

Aster, R., Borchers, B., Thurber, C., 2005. Preface. Int. Geophys. 90, xi–xii.

Bender, M., Dick, G., Ge, M., Deng, Z., Wickert, J., Kahle, H.-G., Raabe, A., Tetzlaff, G., 2011. Development of a GNSS water vapour tomography system using algebraic reconstruction techniques. Adv. Space Res. 47, 1704–1720.

Bevis, M., Businger, S., Herring, T.A., Rocken, C., Anthes, R.A., Ware, R.H., 1992. GPS meteorology: remote sensing of atmospheric water vapor using the global positioning system. J. Geophys. Res.: Atmos. 97, 15787–15801.

Bi, Y., Mao, J., Li, C., 2006. Preliminary results of 4-D water vapor tomography in the troposphere using GPS. Adv. Atmos. Sci. 23, 551–560.

Bosy, J., Rohm, W., Sierny, J., 2010. The concept of the near real time atmosphere model based on the GNSS and the meteorological data from the ASG-EUPOS reference stations. Acta Geodyn. Geomater 7, 157.

Bourjot, L., Romanowicz, B., 1992. Crust and upper mantle tomography in Tibet using surface waves. Geophys. Res. Lett. 19, 881–884.

Champollion, C., Masson, F., Bouin, M.-N., Walpersdorf, A., Doerflinger, E., Bock, O., van Baelen, J., 2005. GPS water vapour tomography: preliminary results from the ESCOMPTE field experiment. Atmos. Res. 74, 253–274.

Degaleesan, S., Dudukovic, M., Pan, Y., 2001. Experimental study of gas-induced liquid-flow structures in bubble columns. AIChE J. 47, 1913–1931.

Flores, A., de Arellano, J.-G., Gradinarsky, L.P., Rius, A., 2001. Tomography of the lower troposphere using a small dense network of GPS receivers. IEEE Trans. Geosci. Rem. Sens. 39, 439–447.

Foelsche, U., Kirchengast, G., 2001. Tropospheric water vapor imaging by combination of ground-based and spaceborne GNSS sounding data. J. Geophys. Res. 106, 221–227.

Guerova, G., Jones, J., Dousa, J., Dick, G., de Haan, S., Pottiaux, E., Bock, O., Pacione, R., Elgered, G., Vedel, H., 2016. Review of the state of the art and future prospects of the ground-based GNSS meteorology in Europe. Atmos. Meas. Tech. 9, 5385.

Hirahara, K., 2000. Local GPS tropospheric tomography. Earth Planets Space 52, 935–939.

Katzberg, S.J., Torres, O., Grant, M.S., Masters, D., 2006. Utilizing calibrated GPS reflected signals to estimate soil reflectivity and dielectric constant: results from SMEX02. Rem. Sens. Environ. 100, 17–28.

Löfgren, J., Haas, R., Scherneck, H.-G., 2011. Sea-level analysis using 100 days of reflected GNSS signals. In: Proceedings of the 3rd International Colloquium-Scientific and Fundamental Aspects of the Galileo Programme, 31 August–2 September 2011, Copenhagen, Denmark.

Lowe, S.T., Zuffada, C., Chao, Y., Kroger, P., Young, L.E., Labrecque, J. L., 2002. 5-cm-Precision aircraft ocean altimetry using GPS reflections. Geophys. Res. Lett. 29.

Martin-Neira, M., 1993. A passive reflectometry and interferometry system (PARIS): application to ocean altimetry. ESA J. 17, 331–355.

Menke, W., 2012. Geophysical Data Analysis: Discrete Inverse Theory,. Academic Press.

Nilsson, T., Gradinarsky, L., 2006. Water vapor tomography using GPS phase observations: simulation results. IEEE Trans. Geosci. Rem. Sens. 44, 2927–2941.

Rius, A., Cardellach, E., Martin-Neira, M., 2010. Altimetric analysis of the sea-surface GPS-reflected signals. IEEE Trans. Geosci. Rem. Sens. 48, 2119–2127.

Rodriguez-Alvarez, N., Bosch-Lluis, X., Camps, A., Vall-Llossera, M., Valencia, E., Marchan-Hernandez, J.F., Ramos-Perez, I., 2009. Soil moisture retrieval using GNSS-R techniques: experimental results over a bare soil field. IEEE Trans. Geosci. Rem. Sens. 47, 3616–3624.

Rodriguez-Alvarez, N., Camps, A., Vall-Llossera, M., Bosch-Lluis, X., Monerris, A., Ramos-Perez, I., Valencia, E., Marchan-Hernandez, J. F., Martinez-Fernandez, J., Baroncini-Turricchia, G., 2011. Land geophysical parameters retrieval using the interference pattern GNSS-R technique. IEEE Trans. Geosci. Rem. Sens. 49, 71–84.

Rohm, W., Bosy, J., 2009. Local tomography troposphere model over mountains area. Atmos. Res. 93, 777–783.

Roussel, N., Frappart, F., Ramillien, G., Darrozes, J., Desjardins, C., Gegout, P., Pérosanz, F., Biancale, R., 2014. Simulations of direct and reflected wave trajectories for ground-based GNSS-R experiments. Geosci. Model Dev. 7, 2261–2279.

Ruffini, N.G., Soulat, F., Caparrini, M., Germain, O., Martín-Neira, M., 2004. The Eddy experiment: accurate GNSS-R ocean altimetry from low altitude aircraft. Geophys. Res. Lett., 31.

Semmling, A.M., Beyerle, G., Stosius, R., Dick, G., Wickert, J., Fabra, F., Cardellach, E., Ribó, S., Rius, A., Helm, A., 2011. Detection of Arctic Ocean tides using interferometric GNSS-R signals. Geophys. Res. Lett. 38.

Thampi, S.V., Yamamoto, M., Tsunoda, R.T., Otsuka, Y., Tsugawa, T., Uemoto, J., Ishii, M., 2009. First observations of large-scale wave structure and equatorial spread F using CERTO radio beacon on the C/NOFS satellite. Geophys. Res. Lett. 36.

Troller, M., Geiger, A., Brockmann, E., Bettems, J.-M., Bürki, B., Kahle, H.-G., 2006. Tomographic determination of the spatial distribution of water vapor using GPS observations. Adv. Space Res. 37, 2211–2217.

Watkins, D., 2002. Fundamentals of Matrix Computations. Jonh Wiley & Sons Inc., New York.

Xia, P., Cai, C., Liu, Z., 2013. GNSS troposphere tomography based on two-step reconstructions using GPS observations and COSMIC profiles. Ann. Geophys. Copernicus GmbH, 1805–1815.

Yang, X., Sass, B.H., Elgered, G., Johansson, J.M., Emardson, T.R., 1999. A comparison of precipitable water vapor estimates by an NWP simulation and GPS observations. J. Appl. Meteorol. 38, 941–956.

Zavorotny, V.U., Voronovich, A.G., 2000. Scattering of GPS signals from the ocean with wind remote sensing application. IEEE Trans. Geosci. Rem. Sens. 38, 951–964.

Zuffada, C., Hajj, G.A., Kursinski, E.R., 1999. A novel approach to atmospheric profiling with a mountain-based or airborne GPS receiver. J. Geophys. Res.: Atmos. 104, 24435–24447.